ELSEVIER

International Journal of Mass Spectrometry 220 (2002) 111–126

International Journal of Mass Spectrometry

www.elsevier.com/locate/ijms

Probing several structures of $Fe(H_2O)_n^+$ and $Co(H_2O)_n^+$ ($n = 1, \ldots, 10$) cluster ions

L. Poisson[1], L. Dukan[2], O. Sublemontier, F. Lepetit, F. Réau, P. Pradel, J.-M. Mestdagh*, J.-P. Visticot

Laboratoire Francis Perrin (CNRS-URA-2453), CEA/DRECAM/Service des Photons, Atomes et Molécules, C.E. Saclay, F-91191 Gif-sur-Yvette Cedex, France

Received 24 September 2001; accepted 25 February 2002

Abstract

$Co(H_2O)_{n\leq 10}^+$ and $Fe(H_2O)_{n\leq 10}^+$ cluster ions were generated in a source combining laser ablation and a supersonic expansion. The clusters were fragmented to get insight into their structure. Two questions were addressed: first, the arrangement of the water molecules about the metal ion, and second, the electronic properties of the solvated metal ion. Collision induced dissociation by helium was used to answer the first question, especially for the smallest clusters with $n = 2$ and 3. This revealed the existence of filament structures where one water molecule lies in the second solvation shell about the metal ion although the first shell is not filled. The binding energies of second shell water in $Co(H_2O)_2^+$ and $Fe(H_2O)_2^+$ are 0.45 ± 0.1 and 0.5 ± 0.1 eV, respectively. The answer to the second question was provided by photofragmentation experiments where the cluster ions are illuminated at 532, 355 and 266 nm. The most striking effect is seen with cobalt ions where increasing the number n of water molecules above $n = 7$ allows one to built up an absorption band that is known when Co^+ is solvated in liquid water. The two fragmentation techniques appear as complementary. (Int J Mass Spectrom 220 (2002) 111–126)

Keywords: Cluster ion; CID; Photofragmentation

1. Introduction

Marinelli and Squires [1] and Magnera et al. [2] were the first groups to report binding energies of a water molecule in $M(H_2O)_n^+$ clusters, where M is a transition metal. The accuracy of these early measurements has been improved in a series of collision induced dissociation (CID) experiments performed in the group of Armentrout and co-workers [3,4]. Moreover, ab initio calculations have been performed by Bauschlicher and co-workers, providing the necessary information on the structure of these clusters [5–7]. Taken together, these works have shown that the most stable configuration of the $M(H_2O)_{n\leq 4}^+$ clusters have the water molecules directly attached to the metal ion.

Our recent work on CID of the $Fe(H_2O)_2^+$, $Co(H_2O)_2^+$ and $Au(H_2O)_2^+$ clusters by helium has shown that an ion source which associates laser ablation and supersonic expansion can generate metastable clusters where one of the water molecules lies in the second solvation shell [8]. The existence of such a

* Corresponding author. E-mail: jmm@drecam.saclay.cea.fr
[1] Present address: Chemical Sciences Division, Lawrence Berkeley Laboratory, 6-2101 ALS LBL, Berkeley, CA 94720, USA.
[2] Present address: Département de chimie, Université de Nice Sophia-Antipolis, C.M.O.M., F-06108 Nice Cedex 2, France.

1387-3806/02/$ – see front matter
PII S1387-3806(02)00684-X

species, where a water molecule is present in the second shell, even though the first shell is not closed, is actually not a surprise. For example, photofragmentation spectra were reported by the group of Fuke for the $Mg(H_2O)_{1-5}^+$ ions [9]. The most stable structure of these ions has up to three water molecules in the first solvation shell, additional water molecules being in outer shells. This corresponds to the dominant isomer responsible for the experimental spectra. Nevertheless shoulders and weak peaks in the spectra have recently been assigned to less stable isomers that are also present in the cluster ion beam [10]. Interestingly, these cluster ions were produced in a source that is comparable to our. Structural isomers of the $Cs(H_2O)_4^+$ cluster have been reported also [11,12].

The present work aims at investigating conformations of the $M(H_2O)_n^+$ cluster ions (M = Co, Fe), where one or several water molecules are located beyond the first solvation shell, although the first solvation shell is not completed. Four families of clusters labeled I_1, I_2, I_3 and $I_{\geq 4}$ will be considered throughout the present paper. They correspond a different number of water molecules in the first shell, respectively, one–four or more. Hence, each family will correspond to a different local environment of the metal ion. Of course, only the isomer family I_1 has to be considered for the $M(H_2O)^+$ cluster ions. Two kinds of isomers I_2 (the most stable one) and I_1 are to be anticipated for the $M(H_2O)_2^+$ cluster ions as observed in our former work when M = Fe, Co and Au [8]. It is useful to recall also that the most stable isomer of the $M(H_2O)_1^+$, $M(H_2O)_2^+$, $M(H_2O)_3^+$, and $M(H_2O)_4^+$ cluster ions, has all the water molecules directly bonded to the metal ion, and consequently corresponds to the isomer family I_1, I_2, I_3 and $I_{\geq 4}$, respectively.

The Smalley type source used in our previous work is again used to generate $Co(H_2O)_{1\leq n\leq 10}^+$ and $Fe(H_2O)_{1\leq n\leq 10}^+$ clusters [8]. Two different experiments are performed to interrogate the structure of the cluster ions produced by this source:

- the first type of experiments is CID, using helium as the target gas. Recent work in our group has shown that molecular dynamics simulations describing the energy transfer between helium and the cluster can be used to extract quantitative information on the water binding energy from CID measurements [13]. The same technique is used here for the data analysis;
- the second type of experiments takes advantage that the visible and close UV electronic excitation of the cluster ions is due to an electronic transition of the core ion. Hence photofragmentation of the clusters at 532, 355 and 266 nm is used to document the water environment about the metal ion. Preliminary results of this type have been reported for the $Fe(H_2O)_{1\leq n\leq 9}^+$ cluster ions [14] and a full discussion will be given here.

2. Experimental

2.1. Apparatus

The apparatus is drawn in Fig. 1. Details can be found in [8,14,15]. Briefly, the cluster beam is produced in a Smalley source where an ablation laser is focused on a metal rod. The ion source is coupled to a pulsed helium/water jet, in order to carry the ions into a supersonic expansion zone. The gaseous mixture cooled by the expansion contains helium (the carrier gas), water which was seeded into helium prior to the expansion, plus neutral atoms and positively charged ions from the metal rod. The desired $M(H_2O)_n^+$ cluster ions are formed and cooled by collisions with helium during the supersonic expansion.[3]

The positively charged species present in the beam are extracted and accelerated to 500 eV, perpendicularly to the beam, using a pulsed Wiley–McLaren TOF-MS. An electrostatic gate follows, allowing us to

[3] Whatever the generating conditions of the cluster beam, the dominant cluster family is $M(H_2O)_n^+$ (M = Fe or Co). Nevertheless, other types of clusters are also present in the beam before mass selection. For instance, the source conditions can be optimized so as the cluster family $M_2(H_2O)_n^+$ is significant [15]. The source also generates cluster ions of the type $MOH(H_2O)_n^+$, but nothing is observed on this cluster family, which is comparable to the product switches encountered for Mg, Ca and Sr which make the $MOH(H_2O)_n^+$ ion family dominant for certain values of n [16–19].

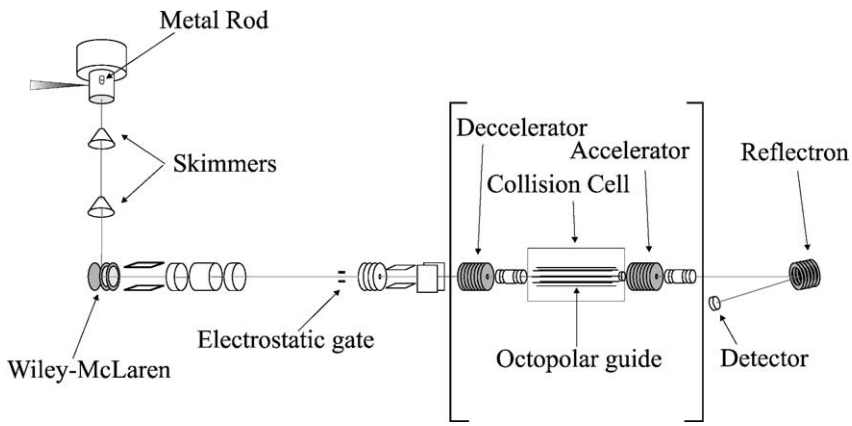

Fig. 1. Schematic view of the apparatus. The assembly between brackets is used for the CID experiments. It is removed for the photofragmentation experiments and is replaced by the crossing zone between the photofragmentation laser and the ion beam.

select the desired cluster ions, $M(H_2O)_n^+$, with M = Fe, Co and $n = 1, \ldots, 10$ in the present work.

2.1.1. The "CID" mode

Downstream the electrostatic gate, an assembly formed by a decelerator, a collision cell and an accelerator is inserted in the ion path for the CID experiments. It is drawn between brackets in Fig. 1. With this device, the cluster ions are decelerated down to an energy ranging between 20 (sometimes 10) and 200 eV in the laboratory frame, then they are collided with helium and partly dissociated in the collision cell. After the collision cell, parent and fragment ions are re-accelerated to the nominal energy. Finally, they enter a reflectron mass spectrometer and are detected. An RF-octopole field guides the cluster ions in the collision cell in order to prevent ion losses. This, together with an accurate determination of both the interaction length and the helium pressure, allows us to determine absolute CID cross-sections. As shown in [15], the CID experiments are run with the Wiley–McLaren device operating under the double extraction mode. This ensures enough mass resolution to the system to distinguish between parent and fragment ions after the collision. However, the mass resolution is not sufficient when the ion energy is brought below 20 eV in the collision cell. Because of this limitation, collision energies can be explored only marginally below 0.5 eV in the center of mass reference frame.

Importantly, the fragment peaks in the mass spectra does not exhibit a tail that would have suggested fragmentation in the acceleration zone, after the clusters have left the collision cell. In other words, we can consider that clusters that carry enough internal energy to dissociate, actually have enough time to do so during the time spent in the collision cell.

2.1.2. The "photofragmentation" mode

The assembly between brackets in the figure is removed and the Wiley–McLaren device is run under the standard single pulse extraction regime. In that case, the photofragmentation laser crosses the cluster beam in the focusing zone of the Wiley–McLaren MS. The light is the second (532 nm), third (355 nm) and and fourth (266 nm) harmonic of a pulsed YAG laser operating at 1.064 μm. Special attention is given to have uniform illumination of the interaction zone between the laser and the ion beam. Moreover, the size of the interaction zone and the timing of the laser pulse are adjusted so the laser pulse matches exactly the ion packet to be photofragmented. This is needed to optimize signal and extract photofragmentation cross-sections quantitatively. After the laser interaction zone, the ions, parents and fragments enter into the reflectron mass spectrometer and are detected.

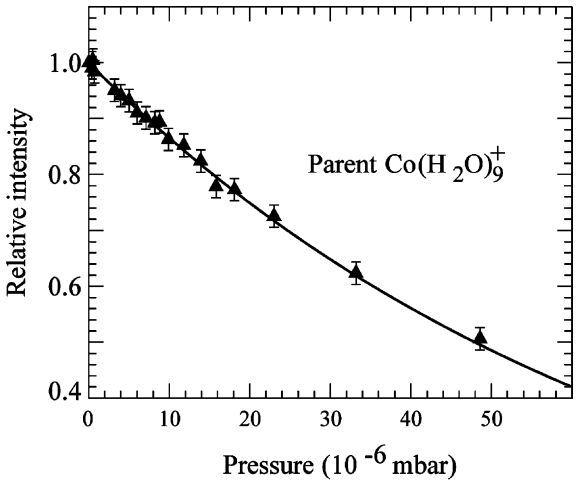

Fig. 2. Relative intensity of the parent ion signal $Co(H_2O)_9^+$ as a function of the helium pressure in the collision cell. The collision energy is 0.76 eV in the center-of-mass reference frame. The full line displays the best fit to the experimental data, using expression (1).

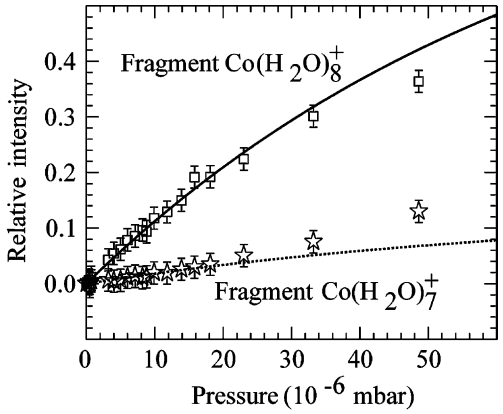

Fig. 3. Relative population of the fragment ions $Co(H_2O)_{7,8}^+$ as a function of the helium pressure in the collision chamber for the collision of $Co(H_2O)_9^+$ with helium at a center-of-mass energy of 0.76 eV. The curves running through the experimental points are the best fits performed using expression (2).

2.2. Cross-section measurements

2.2.1. CID cross-sections

The total CID cross-section have been measured by monitoring the decay of the parent ion signal as a function of the helium pressure in the collision cell. A typical measurement is shown in Fig. 2 for $Co(H_2O)_9^+$ colliding with helium at an energy of 0.76 eV in the center-of-mass reference frame. The relative population N of this ion decays as the helium pressure P is increased. It can be fitted adequately by a single exponential:

$$N = \exp\left(-\sigma \frac{P}{kT} L\right) \quad (1)$$

where T is the temperature of helium in the collision chamber, L the length of the collision chamber and k the Boltzmann constant. This indicates that the parent ion decay results from a single collision process, the cross-section of which is determined by using σ in expression (1) as a parameter to fit the experimental results.

The ion source generates several isomers of the same cluster ion. If the CID cross-sections were very different from one isomer to the other, the parent ion decay should not be reproduced by the monoexponential expression (1) but by a sum of exponentials. No such behavior is observed in Fig. 2. Hence, if several isomers of the $Co(H_2O)_9^+$ cluster are present in the beam, their CID cross-sections are not very different from one isomer to the other at this collision energy.

The fragment ion signals have been monitored also, as a function of the helium pressure. Examples are shown in Fig. 3 for the loss of one and two water molecules in the collision of $Co(H_2O)_9^+$ with helium at a center-of-mass energy of 0.76 eV. Assuming that the single collision regime is achieved, the fragment ion signal N_f is given by

$$N_f = \frac{\sigma_f}{\sigma}\left[1 - \exp\left(-\sigma \frac{P}{kT} L\right)\right] \quad (2)$$

where σ_f is the partial cross-section for forming the fragment f. The other quantities, P, T, L and σ of this expression are defined in expression (1). Expression (2) was used to fit the fragment signals shown in Fig. 3. A good fit is achieved at pressures below 20×10^{-6} mbar, indicating a single collision process. Above this value, the abundance of the $Co(H_2O)_8^+$ cluster ion is smaller than expected for the single collision regime, whereas the abundance of the $Co(H_2O)_7^+$

ion is larger. This is due to secondary collisions which dissociate $Co(H_2O)_8^+$ into $Co(H_2O)_7^+$.

In the present experiment, signals corresponding to all the possible fragments are recorded. The sum of all the partial cross-sections is thus equal to the fragmentation cross-section of the parent ion. This justifies the normalization factor (σ_f/σ) used in expression (2). In practice, as ion losses cannot be avoided totally, the experimental results have been normalized to a constant total ion current when the helium pressure is varied.

2.2.2. Photofragmentation cross-sections

The photofragmentation cross-section is measured by recording the parent ion signal as a function of the fluence Φ_L of the laser. Assuming that the photofragmentation is a single photon process and that a single isomer of the parent ion is present in the beam, a monoexponential decay of the parent ion signal N is expected:

$$N = \exp\left(-\sigma^{ph}\frac{\Phi_L}{h\nu}\right) \quad (3)$$

where $h\nu$ is the photon energy and σ^{ph} the photofragmentation cross-section.

An experimental result is shown in Fig. 4 for the photofragmentation of the $Co(H_2O)_8^+$ cluster ion at 355 nm. The decay is clearly not monoexponential (filled circles). This reveals either the presence of, at least, two populations (A and B) in the beam that are associated with two very different photofragmentation cross-sections, or to hot species associated with a broad distribution of photofragmentation cross-sections. To decide between the two possibilities, the experimental decay of Fig. 4 has been fitted tentatively by a linear combination of two exponentials:

$$N = a\exp\left(-\sigma_A^{ph}\frac{\Phi_L}{h\nu}\right) + (1-a)\exp\left(-\sigma_B^{ph}\frac{\Phi_L}{h\nu}\right) \quad (4)$$

This expression follows the two population assumption. Then, a is the relative population of isomer A, whereas σ_A^{ph} and σ_B^{ph} are the photofragmentation cross-sections of isomers A and B, respectively. The best fit is shown as the solid line in Fig. 4. It indicates that one of the isomers (say isomer B) has a zero, i.e., non-measurable photofragmentation cross-section. Its relative population is $25 \pm 3\%$ before laser irradiation. The good agreement between the experimental points and the best fitting curve in Fig. 4 is a clue, but not a proof yet, that the hot cluster assumption is excluded. To step further, the decay of the laser sensitive population (isomer A) is followed specifically. This is shown in Fig. 4 also. The curve with open circles is obtained by subtracting $25 \pm 3\%$ (i.e., the initial population of isomer B) from the total $Co(H_2O)_8^+$ signal. It thus shows the decay of isomer A alone as the laser fluence is increased. Within error bars, the latter appears as monoexponential (a straight line in the log scale of Fig. 4) over two decades. This strongly supports the assumption that two populations associated with two very different photofragmentation cross-sections (one being close to zero) are present in the beam.

We are thus facing the situation, illustrated by the above $Co(H_2O)_9^+$ data, that several isomers of the $M(H_2O)_n^+$ ions are present in the beam. As recalled in Section 1, this was expected since isomers, assigned to structural isomers, have been observed in several other groups when generating $M(H_2O)_n^+$ clusters in supersonic expansions [9,11,12].

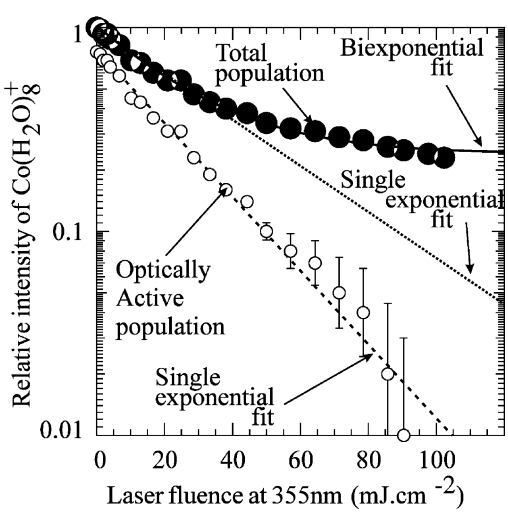

Fig. 4. Decay of the parent ion $Co(H_2O)_8^+$ as a function of the laser fluence in a 355 nm photofragmentation experiment.

Let us do a final remark. Fitting a single ion decay such as that shown in Fig. 4 using a double exponential is always difficult and could result into a very inaccurate determination of the parameters a, σ_A^{ph} and σ_B^{ph}. A way to improve the reliability of the fit is to increase the number of constraints on the fitting parameters. We do this in Section 3.2, where the photofragmentation results are presented.

3. Results

3.1. Collision induced dissociation

3.1.1. The $Fe(H_2O)_{1,2}^+$ and $Co(H_2O)_{1,2}^+$ cluster ions

The CID cross-section of the $Fe(H_2O)_{1,2}^+$ and $Co(H_2O)_{1,2}^+ + He$ collisions have been measured as a function of the center of mass collision energy. The corresponding results are shown in Fig. 5. A preliminary version of these cross-sections appeared already in [8]. However, the present results benefit from an improved procedure for the data acquisition, which yield higher accuracy as those shown for the $Au(H_2O)_{1,2}^+$ ions in [8]. Hence the present $Fe(H_2O)_{1,2}^+$ and $Co(H_2O)_{1,2}^+$ cross-sections deserve the same fancy data analysis procedure than performed in [13] for the $Au(H_2O)_{1,2}^+$ ions.

Poisson et al. [13] report on molecular dynamics calculations that model the energy transfer between helium and cluster ions of the form $M(H_2O)_n^+$. It appears that the initial energy deposition on the cluster is local. Moreover, the amount of energy that is deposited, depends on the mass of the cluster atom that is collided by helium (whether it is H, O or the metal ion). More importantly, this amount depends on whether atom that is hit is involved in an H-bond. It has been shown in [13] how to use these energy transfer calculations to simulate the energy dependence of CID cross-sections, using a single parameter, the binding energy of the water molecule that is to be lost. Otherwise, the only input of the model is the structure of the

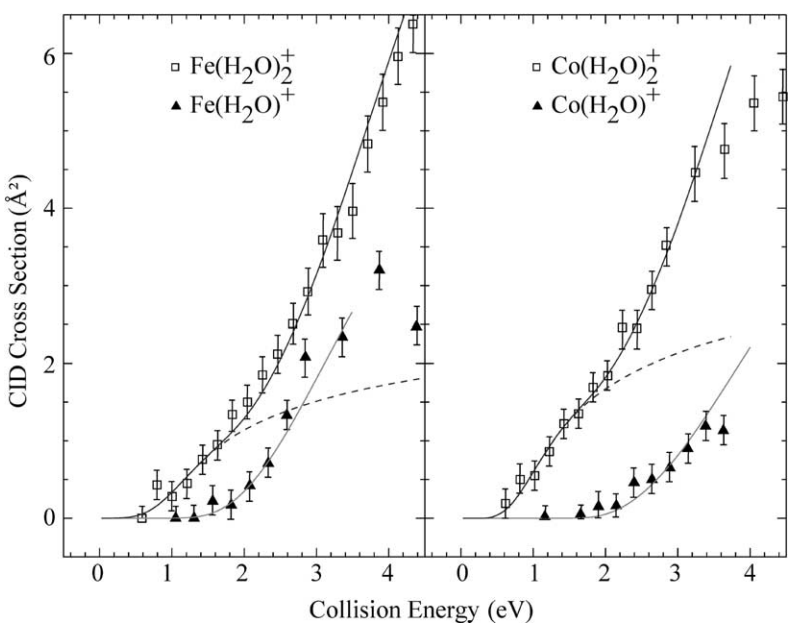

Fig. 5. Energy dependence of the CID cross-section for $Fe(H_2O)_{1,2}^+ + He$ (left panel) and $Co(H_2O)_{1,2}^+ + He$ (right panel) collisions. The solid curves running through the experimental points are simulations based on molecular dynamics calculations as explained in the text. The presence of both a filament (isomer I_1) and a compact (isomer I_2) isomer is assumed in the case of $(Fe,Co)(H_2O)_2^+$. The dashed curve in each panel gives the contribution of the filament isomer to the full cross-sections.

cluster under consideration, i.e., the number of atoms of each kind that are involved in a H-bonding. This allows one indeed to determine the efficiency of the energy transfer. When two isomers are present in the beam, two such cross-sections are summed according to the population ratio between both isomers. This procedure has been applied quantitatively in [13] and has helped to document the compact ($(H_2O)Au^+(H_2O)$) and the filament ($Au^+(H_2O)(H_2O)$) isomers of the $Au(H_2O)_2^+$ cluster ion.

The same procedure is applied here for $Fe(H_2O)_{1,2}^+$ and $Co(H_2O)_{1,2}^+$. There is no fitting parameter to adjust in the model for the $Fe(H_2O)^+$ and $Co(H_2O)^+$ since only one isomer of the ion is present in the beam and the binding energy is known from the experimental work by Armentrout and co-workers [20]. Hence, the solid curve passing through the experimental points in Fig. 5 is not a fit. It is the prediction, based on the molecular dynamics calculation of [13] of both the absolute value and the energy dependence of the CID cross-sections for $Fe(H_2O)^+$ and $Co(H_2O)^+ + He$ collisions. The agreement with the experiment is excellent.[4]

When turning to $Fe(H_2O)_2^+$ and $Co(H_2O)_2^+$, the situation is more complex since two isomers are present in the beam. This has been shown in [8]. One isomer has both water molecules in the first solvation shell and corresponds to the compact structure $(H_2O)M^+(H_2O)$. With the notation defined in Section 1 of the present paper, this isomer is of the I_2 family (two water molecules in the first solvation shell). The other isomer, of the I_1 family, has the filament structure $M^+(H_2O)(H_2O)$ with only one water molecule attached to the metal ion. The binding energy of a water molecule in isomer I_2 is known from the experimental work by Armentrout and co-workers [20]. Therefore, the solid line passing through the experimental points for $Fe(H_2O)_2^+$ and $Co(H_2O)_2^+$ in Fig. 5 is a fit, using only two parameters: the unknown binding energy of the most weakly bonded water molecule in the $M^+(H_2O)(H_2O)$ isomer (I_1) and the population ratio between both isomers. The contribution of the filament isomer is shown as a dashed line in the figure. Though not negligible, its presence does not show up as a step in the energy dependence of the cross-section. This contrasts with the $Au(H_2O)_2^+$ data reported in [13]. In that case, a step associated with the filament isomer was visible because the binding energy of water is very different between the filament and the compact isomers.

[4] This agreement is an indication that the $Fe(H_2O)^+$ and $Co(H_2O)^+$ clusters are cold internally. Otherwise the threshold behavior of the cross-section would be badly reproduced by the calculation.

Table 1
Binding energy of the most weakly bonded water molecule in the $Fe(H_2O)_{1,2}^+$ and $Co(H_2O)_{1,2}^+$ clusters

Cluster	Isomer	Binding energy (eV)	Isomer population (%)
$Fe(H_2O)^+$		1.36[a]	
$Fe(H_2O)_2^+$	I_2	1.70[a]	88 ± 3
$Fe(H_2O)_2^+$	I_1	0.5 ± 0.1[b]	12 ± 3
$Co(H_2O)^+$		1.70[a]	
$Co(H_2O)_2^+$	I_2	1.68[a]	84 ± 2
$Co(H_2O)_2^+$	I_1	0.45 ± 0.1[b]	16 ± 2

[a] See [20].
[b] Present work. The last column shows the relative population of isomers I_1 (filament) and I_2 (compact) in the $Fe(H_2O)_2^+$ and $Co(H_2O)_2^+$ beams.

The binding energies and the population ratios used to simulate the CID cross-sections of Fig. 5 are listed in Table 1.

3.1.2. The $Co(H_2O)_{>2}^+$ cluster ions

The total CID cross-section of $Co(H_2O)_n^+$ clusters has been measured as a function of the collision energy. The corresponding results are shown in Fig. 6 for n ranging between 1 and 10. The results corresponding to $n = 6$ and 7 have been omitted for the clarity of the figure, they lead to intermediate situations between $n = 5$ on one hand and $n = 8$, 9, 10 on the other.

The cross-sections measured for $Co(H_2O)_{1,2}^+$ are those reported in Fig. 5. They are an order of magnitude smaller than those measured for the larger clusters. Because of experimental limitations, the cross-sections could not be explored below 0.5 eV. As a result, the threshold region of the CID cross-section could not be explored for the larger clusters. However,

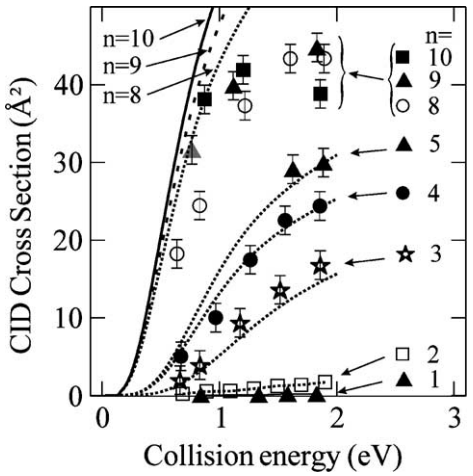

Fig. 6. Energy dependence of the CID cross-section for the $Co(H_2O)_n^+ + He$ collisions. The value of n is ranging from 1 to 10 as labeled in the figure (no experimental result is not reported for $n = 6$ and 7 for clarity). The curves running through the experimental points is a simulation based on molecular dynamics calculations as explained in the text.

the threshold energy seems smaller than 0.5 eV for all the clusters carrying more than two water molecules. This question is re-examined in Section 4 when analyzing the experimental data with the help of the model developed in [13] which describes the collisional energy transfer between helium and the cluster ion.

We know that the cluster beam contains several isomers of the same cluster ion but, as mentioned in Section 2.2, the CID cross-sections associated with the various isomers are not very different from one isomer to the other (except for $Co(H_2O)_2^+$ which has been treated separately). As a result, the cross-sections presented in Fig. 6 must be considered as an average over the isomer distribution.

3.2. Photofragmentation

Irradiation at 532 nm leads to barely observable fragmentation and is not presented further. Measurable photofragmentation is observed for the $Co(H_2O)_{1-10}^+$ and $Fe(H_2O)_{1-10}^+$ cluster ions at 355 and 266 nm where complete data have been recorded. Figs. 7 and 8 show examples of the results: the photofragmentation of $Co(H_2O)_2^+$ and $Co(H_2O)_8^+$ at 266 nm in Fig. 7 and that of $Co(H_2O)_8^+$ at 355 nm in Fig. 8. The parent ion decay is shown in both figures, together with the appearance of the major fragments and reaction products. The decay of the parent show a "non-zero" slope at low laser fluences, indicating that it results from a single photon process. Such a single photon process would lead also to a linear increase of both the fragment and reaction product population at small fluences. This is clearly the case in Fig. 7, when considering either the Co^+ fragment in the $Co(H_2O)_2^+$ photofragmentation or the $Co(H_2O)_2^+$ fragment coming from $Co(H_2O)_8^+$. These fragmentation channels can therefore be assigned to single photon processes. In contrast the Co^+ fragment originating from the $Co(H_2O)_8^+$ photofragmentation cannot be assigned to a single photon event. The decay of the $Co(H_2O)_2^+$ fragment above 30 mJ cm^{-2} is also due to multiphoton processes, where the $Co(H_2O)_2^+$ fragment absorbs a second photon and dissociates as $Co(H_2O)^+$ when $Co(H_2O)_8^+$ is photofragmented at 266 nm. Similar observations can be seen Fig. 8. In the following, we concentrate only on single photon processes.

The $Co(H_2O)_8^+$ decay at 355 nm shown in Fig. 8 appeared at a different scale in Fig. 4. As when presenting the latter figure, the main difference between a CID experiments and photofragmentation is that photofragmentation cross-sections are substantially different from one isomer to the other. The example shown in Fig. 4 indicates that at least two kind of isomers of the $Co(H_2O)_8^+$ cluster are present in the beam. Two of them are dominant, one having a much larger cross-section than the other. The photofragmentation data in the present work, such those reported in Figs. 7 and 8, do not give evidence that more than two isomers participate to the signals observed. Hence for simplicity, the fit to the experimental results for providing photofragmentation cross-sections has been done using expression (4) which assumes the presence of two isomers only. Three parameters then must be fitted, the population ratio between the isomers, and the two photofragmentation cross-sections. As stressed in Section 2.2, extreme attention has to be given to the fitting procedure in order to get meaningful

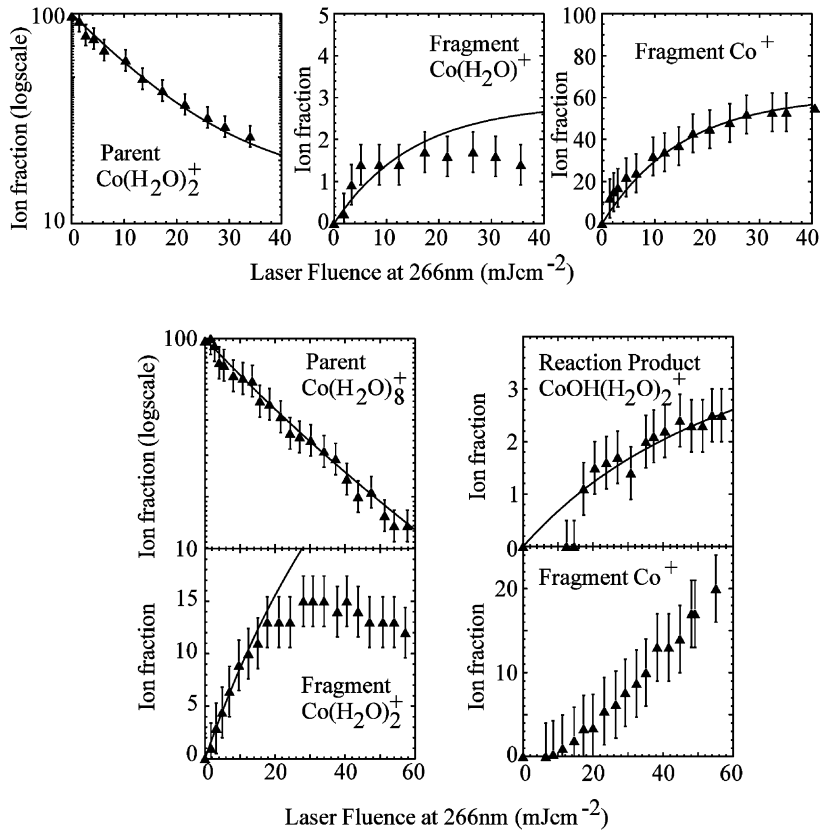

Fig. 7. Decay of the parent ion and appearance of both the fragments and reaction products in the photofragmentation of $Co(H_2O)_2^+$ and $Co(H_2O)_8^+$ at 266 nm. The fraction of each ion is displayed (in percent) as a function of the laser fluence. The solid lines running through the experimental points are fits, assuming that photofragmentation is a single photon process. See the text for details.

cross-sections and several guidelines have been followed to improve the reliability of the fit.

For reasons that will become clear in Section 4.2, the photofragmentation cross-sections are expected to be sensitive to the local environment about the metal ion, i.e., to the number of water molecules that are directly bonded to the metal. The isomers that need to be considered here are the four families I_1, I_2, I_3 and $I_{\geq 4}$ defined in Section 1 of the present paper, which correspond, respectively, to one–four or more water molecules bonded to the metal ion directly.

Figs. 9 and 10 display the photofragmentation cross-sections deduced from the fits of the $Co(H_2O)_n^+$ and $Fe(H_2O)_n^+$ data, as a function of n, for n between 1 and 10. The top panel in each figure corresponds to the 355 nm irradiation and the bottom panel to the 266 nm irradiation. The line going through the points is only for guiding the eyes to each isomer. The quality of the fits is exemplified in Figs. 7 and 8, where they are shown as solid lines. The same isomer ratio was naturally used to fit both the 266 and the 355 nm experiments. Details on the fit are examined below.

3.2.1. $Co(H_2O)_n^+$ at 266 nm

The set of isomers that were needed to fit the $Co(H_2O)_n^+$ data at 266 nm laser excitation is the following: (I_1, I_2) for $Co(H_2O)_2^+$, (I_2, I_3) for $Co(H_2O)_3^+$ and (I_3, $I_{\geq 4}$) for $Co(H_2O)_{6-8}^+$. Only one isomer population was needed in the following cases: I_1 for $Co(H_2O)^+$, I_3 for $Co(H_2O)_{4,5}^+$ and $I_{\geq 4}$

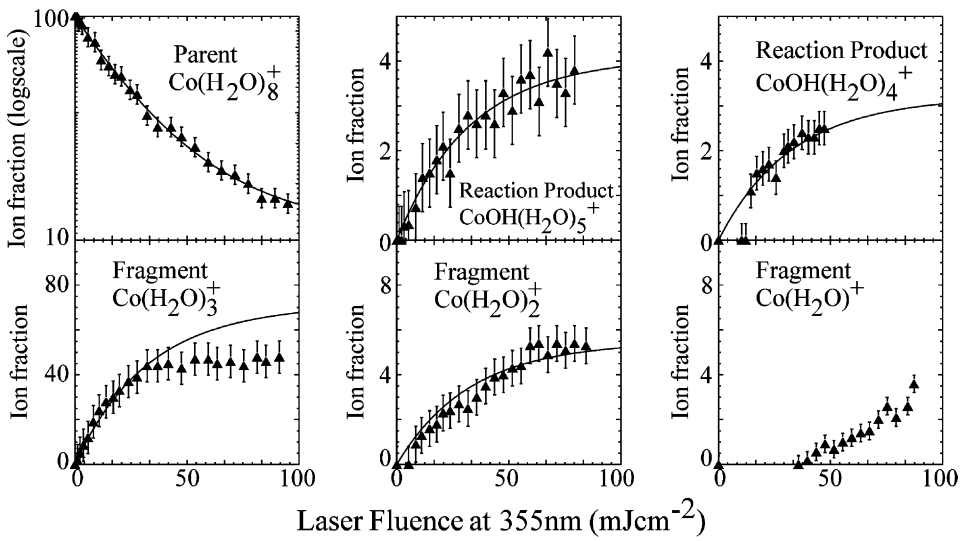

Fig. 8. Same caption as in Fig. 7 for the photofragmentation of $Co(H_2O)_8^+$ at 355 nm.

for $Co(H_2O)_{9,10}^+$. This is summarized in Table 2 together with the fitting parameters that are examined now.

The population ratio between isomers I_1 and I_2 when fitting the $Co(H_2O)_2^+$ data was forced to that found in the CID experiment, otherwise, population ratios were used as parameters to fit the photofragmentation data. The same cross-section has been found for both $Co(H_2O)_9^+$ and $Co(H_2O)_{10}^+$ (0.8×10^{-17} cm^2), where only isomer $I_{\geq 4}$ contributes to the fragmentation. This value has been assumed to be the same for

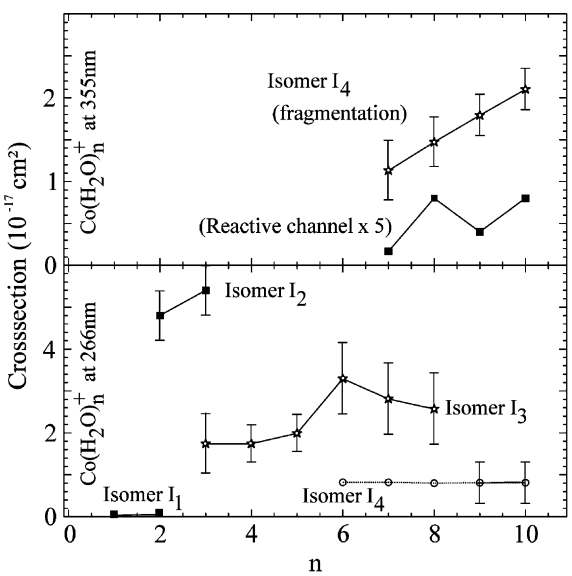

Fig. 9. Photofragmentation cross-section of the various isomers of the $Co(H_2O)_n^+$ cluster ions at 266 and 355 nm as a function of the number of water molecule n.

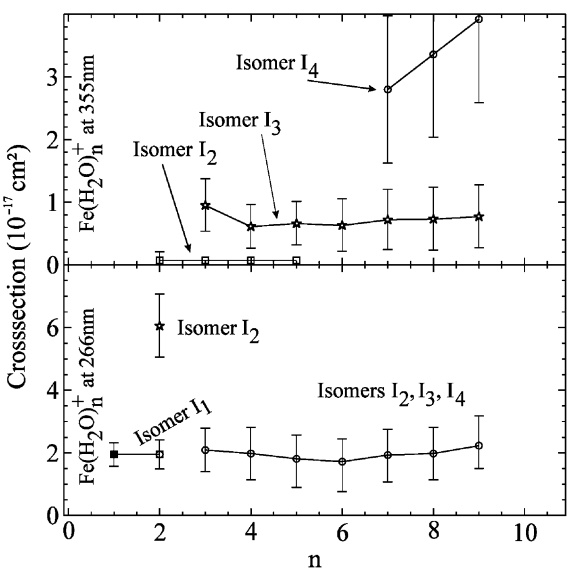

Fig. 10. Same caption as Fig. 9 for the $Fe(H_2O)_n^+$ cluster ions.

isomer $I_{\geq 4}$ when contributing to the $Co(H_2O)_{6,7,8}^+$ photofragmentation together with the isomer I_3. Of course, another choice could have been done. Nevertheless, the assumption of two isomers associated with two significantly different cross-sections is needed to fit the experimental data. The large error bars in Fig. 9 reflects the difficulty of the fits.

The 266 nm excitation leads also to a reactive channel forming $CoOH(H_2O)_p^+$ ions from $Co(H_2O)_{8-10}^+$. The corresponding cross-section is very small ($<0.2 \times 10^{-17}$ cm^2) and is not discussed any further.

3.2.2. $Co(H_2O)_n^+$ at 355 nm

The top panel of Fig. 9 and Table 2 indicates a non-measurable photofragmentation cross-section when the $Co(H_2O)_n^+$ clusters carry less than six water molecules. A barely measurable photofragmentation cross-section $\approx 10^{-18}$ cm^2, could be observed for $n = 6$. It is not reported in the figure and as any the significant cross-sections are shown. Both fragmentation and reaction forming $CoOH(H_2O)_p^+$ ions are observed. The fitting parameters reported in Table 2 indicate that a single isomer has a non-zero photofragmentation cross-section, although two isomers of the $Co(H_2O)_{7,8}^+$ clusters are present in the beam. From the 266 nm experiment, we know that the two isomers present when $n = 7$, 8 are I_3 and $I_{\geq 4}$ and that only $I_{\geq 4}$ is present for $n = 9$ and 10. Hence, the isomer that has a non-zero photofragmentation cross-section in the 355 nm experiment is assigned to $I_{\geq 4}$.

3.2.3. $Fe(H_2O)_n^+$ at 266 nm

Except for the $Fe(H_2O)_2^+$ ion, where the population ratio between isomer I_1 and I_2 was taken from the CID experiment, all the photofragmentation data could be fitted with a single population. Since several isomers of the type I_3 and $I_{\geq 4}$ are probably present in the cluster beam for $n \geq 3$, this is an indication that they have comparable cross-sections at 266 nm.

A reactive channel is also observed for the $Fe(H_2O)_{5,7,8}^+$ clusters. Again, its cross-section was always smaller than 10^{-18} cm^2 and is not reported in the figure.

3.2.4. $Fe(H_2O)_n^+$ at 355 nm

Except for the $Fe(H_2O)_2^+$ ion, where the population ratio between isomer I_1 and I_2 was taken from the CID experiment, no population ratios between the $Fe(H_2O)_n^+$ isomers could be double checked. As a result, the cross-section given in the top panel of Fig. 10 are indicative, and the error bars are given accordingly. The following trend can be drawn: isomer I_1 is necessarily the only one present in experiments with $Fe(H_2O)^+$. It does not absorb the 355 nm light, as the photofragmentation cross-section is zero. The

Table 2
Photofragmentation cross-section and population ratios between isomers used to fit the photofragmentation data of the $Co(H_2O)_n^+$ cluster ions

Cluster	Isomers[a]											
	I_1 ($\times 10^{-17}$ cm^{-2})			I_2 ($\times 10^{-17}$ cm^{-2})			I_3 ($\times 10^{-17}$ cm^{-2})			$I_{\geq 4}$ ($\times 10^{-17}$ cm^{-2})		
	%	266 nm	355 nm	%	266 nm	355 nm	%	266 nm	355 nm	%	266 nm	355 nm
$Co(H_2O)^+$	100	N	N									
$Co(H_2O)_2^+$	**16**	N	N	**84**	5	N						
$Co(H_2O)_3^+$				70	5.4	N	30	1.7	N			
$Co(H_2O)_4^+$							100	1.7	N			
$Co(H_2O)_5^+$							100	2.0	N			
$Co(H_2O)_7^+$							55	2.8	N	45	**0.8**	1.1
$Co(H_2O)_8^+$							25	2.6	N	75	**0.8**	1.5
$Co(H_2O)_9^+$										100	0.8	1.8
$Co(H_2O)_{10}^+$										100	0.8	2.1

The boldface parameters have not been adjusted but are taken from other measurements as explained in the text. N means non-measurable.

non-zero cross-sections that are fitted for the larger clusters suggest a step by step increase when switching from I_2 to I_3 and to $I_{\geq 4}$. This suggests an enhanced absorption of the 355 nm light by the Fe^+ chromophore when more water molecules are ligated to the iron ion. No reactive channel assignable to a single photon process is observed at 355 nm.

4. Discussion

4.1. CID experiments

4.1.1. $Co(H_2O)_{1,2}^+$ and $Fe(H_2O)_{1,2}^+$ clusters

The energy dependence of the CID cross-sections shown in Fig. 5 have been fully interpreted in Section 3.1. When passing through the experimental points, the curve predicts the absolute value and the energy dependence of the CID cross-section. The output was in full consistency with the experimental data of Armentrout and co-workers both for $Co(H_2O)^+$ and $Fe(H_2O)^+$, and for the compact isomer I_2 of $Co(H_2O)_2^+$ and $Fe(H_2O)_2^+$ [20]. The new data brought by the present work is the binding energy of the outer water molecule in the filament isomer I_1 of $Co(H_2O)_2^+$ and $Fe(H_2O)_2^+$, respectively, 0.45 ± 0.1 and 0.50 ± 0.1 eV as read in Table 1. These values replace the less accurate determination of 0.7 ± 0.2 eV given in our former work [8].

4.1.2. $Co(H_2O)_3^+$ clusters

The data analysis used for the $Co(H_2O)_2^+$ and $Fe(H_2O)_2^+$ cluster can be applied again to interpret the data for $Co(H_2O)_3^+$ in Fig. 6. We know from the photofragmentation experiment that two isomers of the types I_2 and I_3 are present in the beam for this cluster, in the ratio 70:30. Isomer I_3 with the three water molecules in the first solvation shell is the most stable one [4]. It is remarkable to observe that this isomer is less populated than the other. This is the indication that the very intense cooling during the supersonic expansion can stabilize an out of equilibrium situation where abundances are better controlled by the kinetics of the cluster formation than by thermodynamics. This will be encountered again with the $Co(H_2O)_4^+$ clusters.

The binding energy of water in the isomer I_3, has been measured by Armentrout and co-workers at 0.67 ± 0.05 eV [4]. The binding energy of the other isomer is yet unknown. It corresponds to the binding energy of water in the second solvation shell. It can tentatively be assigned to 0.45 eV as for the second shell water molecule in $Co(H_2O)_2^+$. The resulting prediction of the CID cross-section is shown in Fig. 6 as a solid curve. It is in fair agreement with the experiment, indicating that the binding energy of second shell water in $Co(H_2O)_3^+$ is actually close to 0.45 eV. Within the experimental uncertainties, the calculated curve slightly underestimate the measured cross-section, indicating that the binding energy of water is slightly smaller than 0.45 eV. This result is reported in Table 3 which summarizes the information on the water binding energy in the $Co(H_2O)_n^+$ cluster ions.

4.1.3. $Co(H_2O)_{>3}^+$

When applied to the larger clusters, the data analysis procedure becomes less and less accurate, in particular because the smallest collision energy that could be explored is 0.5 eV. It has been applied nevertheless to get a trend on the water binding energy.

The situation is quite simple for $Co(H_2O)_{4,5}^+$ clusters where the photodissociation experiment reveal a

Table 3
Binding energy in eV of a water molecule in the $Co(H_2O)_n^+$ clusters, according to their location in the first solvation shell, the second one of beyond

Cluster	First shell	Second shell	Beyond second shell
$Co(H_2O)^+$	1.70 ± 0.06[a]		
$Co(H_2O)_2^+$	1.68 ± 0.07[a]	0.45 ± 0.1[b]	
	Isomer I_2	Isomer I_1	
$Co(H_2O)_3^+$	0.67 ± 0.05[a]	$\lessapprox 0.45$[b]	
	Isomer I_3	Isomer I_2	
$Co(H_2O)_4^+$	0.60 ± 0.06[a]	0.35 ± 0.1[b]	
	Isomer $I_{\geq 4}$	Isomer I_3	
$Co(H_2O)_5^+$		0.35 ± 0.1[b]	
		Isomer I_3	
$Co(H_2O)_{>8}^+$			$\gtrapprox 0.23$[b]
			Isomer $I_{\geq 4}$

[a] See [3,4].
[b] Present work.

single isomer of the type I_3.[5] CID of these clusters then yield information on the binding energy of a second shell water molecule. The best fit to the experimental data is shown as the solid line through the experimental points in Fig. 6 and corresponds to the binding energies of 0.35 eV reported in Table 3 for $Co(H_2O)_4^+$ and $Co(H_2O)_5^+$. When combined with the results on $Co(H_2O)_3^+$, the trend is a decrease of the binding energy of second shell water molecule when the size of the cluster increases.

For the largest clusters, $Co(H_2O)_{8,9,10}^+$, the photofragmentation data indicate that isomer with four or more water molecules in the first solvation shell, $I_{\geq 4}$, is dominant. The structure of these ions is very difficult to anticipate, in particular the number of water molecules present in the first solvation shell. Only theoretical investigations could answer this question. Tentatively, we assume that the loss of a water molecule by these ions corresponds to a loss beyond the second shell. In that case, the ion charge is likely to be screened completely by the water molecules of the first two shells, and the binding energy of a water molecule beyond the second shell should be close to the water–water binding energy in the water dimer (a pure H-bond). The latter was measured as 0.23 ± 0.01 eV in [21,22] and calculated to be 0.21 eV [23–25]. A value of 0.23 eV has been assumed for the water binding energy to simulated the CID cross-section of the $Co(H_2O)_{8,9,10}^+$ clusters in the molecular dynamics simulation. The corresponding curves are reported in Fig. 6. They overestimate slightly the experimental cross-section indicating a slightly larger binding energy of water than assumed in the calculation.

4.2. Photofragmentation experiments

The photofragmentation data presented in Section 3.2 have been analyzed with the assumption that one or two types of the isomers labeled I_1, I_2, I_3 or $I_{\geq 4}$ are present in the $Fe(H_2O)_n^+$ and $Co(H_2O)_n^+$ cluster ion beams. When the same cluster ion exists with two isomeric forms, the corresponding photofragmentation cross-sections appear often very different (see Figs. 9 and 10 and Table 2). Such behavior was expected and was one of the motivations of the present work. It is linked to the fact that the absorption band of the solvated Fe^+ and Co^+ ions is strongly dependent on the ion electronic structure which itself is likely to be affected by the metal ion environment. In particular, changes in the first solvation shell are likely to induce dramatic perturbations in the ion electronic levels. A striking example is the spin flip from sextet to quartet that occurs in Fe^+ when switching from one to two water molecules in the first solvation shell [5]. In contrast, changes in outer solvation shell are not expected to induce such drastic perturbations of the ion core, except when charge transfer phenomena begin to take place.

These considerations serve as a framework to discuss the photofragmentation results. Cobalt and iron are discussed separately.

4.2.1. $Co(H_2O)_n^+$

The photofragmentation cross-section of $Co(H_2O)^+$ is non-measurable, regardless of the laser wavelength, 532, 355 or 266 nm, an indication that the cluster has likely no absorption band near 2.33, 3.49 and 4.66 eV. Otherwise indeed, the absorption of such electronic energy should result into the fragmentation of the cluster within the time window of the experiment. This result is actually not surprising when considering that the dipole allowed transition of lowest energy is the $3d^8a^3F \rightarrow 3d^7(a^4F)4pz^3G^0$ of Co^+ multiplet, the longest wavelength of which is 206 nm [26]. The present result simply indicates that solvation by one water molecule is not enough either to bring a line of the $3d^8a^3F \rightarrow 3d^7(a^4F)4pz^3G^0$ multiplet up to 266 nm, or to perturb the electronic structure of Co^+ so as to drop the selection rules that prevent transitions to lower electronic states.

Two isomers of $Co(H_2O)_2^+$ are present in the beam. From the CID experiment we know that one is a filament structure with only one water molecule in the first solvation shell (isomer I_1). It is assigned in Fig. 9

[5] As seen above for the $Co(H_2O)_3^+$ cluster, but to a larger extent here, the supersonic expansion produces dominantly an isomer, I_3 that is less compact than the one expected from thermodynamics ($I_{\geq 4}$)

as the isomer that has a non-measurable photofragmentation cross-section at 266 nm simply because its local environment about the ion is close to that of the $Co(H_2O)^+$ cluster which has a zero photofragmentation cross-section at 266 nm. Hence the other isomer, with a quite large photofragmentation of 4.8×10^{-17} cm^2 at 266 nm, must be assigned to the compact isomer I_2 with the two water molecules directly bonded to the metal ion. Such a large cross-section indicates that the additional water molecule has changed the Co^+ electronic configuration substantially so as its resonance transition overlaps the 266 nm excitation.

The photofragmentation data for $Co(H_2O)_3{}^+$ were fitted with two populations, none of which has a zero cross-section at 266 nm. For this reason, none of these populations have been assigned to isomer I_1 in Fig. 9, but to I_2 and I_3. By analogy with the $Co(H_2O)_2{}^+$ results, the largest cross-section for the $Co(H_2O)_3{}^+$ cluster has been assigned to the isomer I_2. The same *continuity rule* has been applied when assigning the 266 nm cross-sections to isomers I_3 and $I_{\geq 4}$ for the $Co(H_2O)_{>6}{}^+$ cluster ions. The trend is a zero cross-section at 266 nm for the isomer I_1, a sharp raise for I_2 and a slow decrease when switching from I_3 to $I_{\geq 4}$. This can be interpreted as a resonance absorption of Co^+ that is red shifted across the laser line at 266 nm and which becomes broader as the number of water molecules solvating the ion gets larger. A similar behavior has been observed by Fuke and co-workers for the $Mg(H_2O)_{1-5}{}^+$ and $Ca(H_2O)_{1-6}{}^+$ clusters [9,18].

More interesting are the results at 355 nm. A monotonically increasing cross-section is observed for $Co(H_2O)_{7,8,9,10}{}^+$. It has been assigned to the isomer $I_{\geq 4}$. The isomer I_3 which is also present in the $Co(H_2O)_{7,8}{}^+$ experiments with significant population (55 and 25%, respectively) has a zero photofragmentation cross-section. We are facing a situation where only the isomer $I_{\geq 4}$, leads to a non-zero cross-section at 355 nm, which further increases when adding more and more water molecules.[6] This result is puzzling since 355 nm is very far from the $3d^8a^3F \rightarrow 3d^7(a^4F)4pz^3G^0$ resonance transition of Co^+ and corresponds to an energy region of parity forbidden transitions [26].

When considering the isomer $I_{\geq 4}$ of larger and larger clusters, rather than discussing solvation as a perturbation of the gas phase Co^+ ion, an attractive alternative is a comparison with liquid phase absorption bands.

The 355 nm absorption observed in the present work may have the same origin as the 370 nm absorption band of Co^+ observed in liquid water [27,28]. The molar absorption coefficient of Co^+ in liquid water is 2080 L mol^{-1} cm^{-1} [29], a value that could not be assigned to a charge transfer band in [27]. It is more likely due to an electronic transition that is vibronically allowed (see [30,31]) in a non-centrosymmetrical structure, most probably a tetrahedral structure enabling the $t_{2g}^4e_g^4 \rightarrow t_{2g}^5e_g^3$ transition.

Nevertheless, the 355 nm excitation turns on the reaction forming $CoOH^+$ in the $Co(H_2O)_{>6}{}^+$ cluster (see Fig. 9). Such a reaction can be viewed as a photoinduced redox reaction since the product $CoOH^+$ can be written under the form $Co^{2+}OH^-$. This is a clue that charge transfer participates slightly in the 355 nm absorption. A charge transfer band from Co^+ to water is described indeed in liquid water at approximatively 315 nm [29]. In the cluster context, it would correspond to a dissociative attachment of the excited Co^+ electron towards the water molecules, resulting in the destabilization of an H atom and formation of the OH^- ion which is stabilized as the product $CoOH^+$. Such a photoinduced electron transfer reaction has been suggested for Co^+ in liquid water from a pulsed radiolysis experiment [32]. Intracluster electron transfer reactions have also been observed in the group of Fuke for $Mg(H_2O)_{n\geq 6}{}^+$ and $Ca(H_2O)_{n\geq 5}{}^+$ clusters [33–35].

4.2.2. $Fe(H_2O)_n{}^+$

Photofragmentation of the $Fe(H_2O)_n{}^+$ clusters has appeared in a preliminary report [14]. It is revisited in Fig. 10 in light of the present results on cobalt. In particular, the data analysis summarized in Fig. 10

[6] A similar behavior, but with two orders of magnitude smaller cross-sections was observed at 532 nm. The corresponding results are not reported here.

included the possibility of several isomers present in the beam in order to account for very slight biexponential decays (especially in the 355 nm experiments) that were disregarded in our former work. Of course, as done before for cobalt, the population ratio between isomers I_1 and I_2 provided by the CID experiment were used to analyze the photofragmentation data of the $Fe(H_2O)_2^+$ clusters.

The enhanced cross-section for $Fe(H_2O)_2^+$ in the 266 nm observed in Fig. 10 has been reported and interpreted already in [14]. The difference with the present data analysis, is that it is assigned to the local environment of the iron ion rather than simply to the cluster. The enhanced cross-section is now assigned to isomer I_2 with two water molecules directly attached to the metal ion. This supports the discussion given in [14] that the large cross-section for $Fe(H_2O)_2^+$ is not simply due to a shift of the resonance transition $Fe^+(3d^6(a^5D)4sa^6D \rightarrow 3d^6(a^5D)4pz^6D)$ from 260 to 266 nm but also to a spin change from sextet to quartet when two water molecules solvate the iron ion [5]. The filament isomer I_1 of $Fe(H_2O)_2^+$, with only one water molecule directly attached to the metal ion, likely belongs in the sextet multiplicity and has a small cross-section as does $Fe(H_2O)^+$. In contrast, isomer I_2 has the two water molecules attached to the metal ion and belongs to the quartet multiplicity. In addition to this spin exchange, a red shift of the resonant transition is also expected. Therefore, the small cross-section for $Fe(H_2O)_{>2}^+$ can be assigned to excite the blue tail of the absorption band after it has been red shifted below 266 nm by the solvation.

We now turn to the 355 nm results. A steep increase of the cross-section is observed. It is zero for $Fe(H_2O)^+$ and becomes larger and larger for the isomers I_2, I_3 and $I_{\geq 4}$. In addition, a continuous increase of the cross-section is observed for isomer $I_{\geq 4}$ when switching from $Fe(H_2O)_7^+$ to $Fe(H_2O)_9^+$. This behavior is reminiscent to that observed for cobalt, which was discussed with the help of liquid phase absorption spectroscopy. Unfortunately, to our knowledge, no information exists in the literature on the Fe^+ ion in solution. It could be imagined that the enhancing cross-section observed for the isomer $I_{\geq 4}$, when the number of water molecules increases from 7to 9, might be due to a photoinduced charge transfer, as already discussed for cobalt. The exact position of this band is not documented in the liquid phase. However, it should fall in the range 300–315 nm as observed for other monocations of the transition metal, Zn^+, Ni^+, Co^+ and Cd^+ [29]. Such a location is consistent with the present results at 355 nm.

5. Concluding remarks

A laser ablation source, coupled to a supersonic expansion, has been used in the present work to form $Co(H_2O)_n^+$ and $Fe(H_2O)_n^+$ cluster ions with n ranging between 1 and 10. These ions have been fragmented in two different ways. One is CID with helium and the other photofragmentation at 532, 355 and 266 nm. The mechanism transferring energy into the cluster is very different in each case, hence the fragmentation mechanism is different, and the information provided on the cluster is complementary.

In short, the CID yields information about:

- the interaction with the target gas (not examined here);
- the outer structure of the cluster. For the $Co(H_2O)_2^+$ and $Fe(H_2O)_2^+$ clusters, CID has informed whether both water molecules are in the first solvation shell or not. In fact two types of isomers have been observed one with both water molecules in the first shell and the second with one water molecule in the second shell. The population ratio between both isomers has been determined. A similar information has been brought on the $Co(H_2O)_3^+$ clusters showing that two types of isomers coexist in the beam, one with the three water molecules in the first shell and the other with a water molecule in the second shell;
- the binding energy of the water molecules to the cluster. Not surprisingly, this allowed us to show that the binding energies of water are weaker beyond the first solvation shell.

In contrast, photofragmentation experiments document the close environment of the ion core. In particular, by localizing the absorption bands of the $Co(H_2O)_n^+$ and $Fe(H_2O)_n^+$ cluster ions, these experiment give indications on the electronic structure of the core ion. It has been interesting to observe an absorption band which is known for Co^+ ion solvated in liquid water, which built up progressively when increasing the number n of water molecules in the $Co(H_2O)_n^+$ clusters above $n = 7$.

References

[1] P.J. Marinelli, R.R. Squires, J. Am. Chem. Soc. 111 (1989) 4101.
[2] T.F. Magnera, D.E. David, D. Stulik, R.G. Orth, H.T. Jonkman, J. Michl, J. Am. Chem. Soc. 111 (1989) 5036.
[3] R.H. Schultz, P.B. Armentrout, J. Phys. Chem. 97 (1993) 596.
[4] N.F. Dalleska, K. Honma, L.S. Sunderlin, P.B. Armentrout, J. Am. Chem. Soc. 116 (1994) 3519.
[5] M. Rosi, C.W. Bauschlicher Jr., J. Chem. Phys. 90 (1989) 7264.
[6] M. Rosi, C.W. Bauschlicher Jr., J. Chem. Phys. 92 (1990) 1876.
[7] A. Ricca, C.W. Bauschlicher Jr., J. Phys. Chem. 99 (1995) 9003.
[8] L. Poisson, P. Pradel, F. Lepetit, F. Réau, J.M. Mestdagh, J.P. Visticot, Eur. Phys. J. D 14 (2001) 89.
[9] F. Misaizu, M. Sanekata, K. Fuke, S. Iwata, J. Chem. Phys. 100 (1994) 1161.
[10] H. Watanabe, S. Iwata, J. Chem. Phys. 108 (1998) 10078.
[11] C.J. Weinheimer, J.M. Lisy, J. Chem. Phys. 105 (1996) 2938.
[12] J.M. Lisy, Int. Rev. Phys. Chem. 16 (1997) 267.
[13] L. Poisson, P. de Pujo, V. Brenner, A.-L. Derepas, J.-P. Dognon, J.-M. Mestdagh, J. Phys. Chem. 106 (2002) 1714.
[14] L. Dukan, L. Del Fabbro, P. Pradel, O. Sublemontier, J.M. Mestdagh, J.P. Visticot, Eur. Phys. J. D 3 (1998) 257.
[15] O. Sublemontier, L. Poisson, P. Pradel, J.-M. Mestdagh, J.-P. Visticot, J. Am. Soc. Mass Spectrom. 11 (2000) 160.
[16] A.S. Harms, S.N. Khanna, B. Chen, A.W. Castleman Jr., J. Chem. Phys. 100 (1994) 3540.
[17] M. Sanekata, F. Misaizu, K. Fuke, S. Iwata, K. Hashimoto, J. Am. Chem. Soc. 117 (1995) 747.
[18] M. Sanekata, F. Misaizu, K. Fuke, J. Chem. Phys. 104 (1996) 9768.
[19] D.C. Sperry, A.J. Midey, J.I. Lee, J. Qian, J.M. Farrar, J. Chem. Phys. 111 (1999) 8469.
[20] N.F. Dalleska, K. Honma, L.S. Sunderlin, P.B. Armentrout, J. Am. Chem. Soc. 116 (1994) 3519.
[21] L.A. Curtiss, D.J. Frurip, M. Blander, J. Chem. Phys. 71 (1979) 2703.
[22] J.R. Reimers, R.O. Watts, M.L. Klein, Chem. Phys. 64 (1982) 95.
[23] S.S. Xantheas, J. Chem. Phys. 102 (1995) 4505.
[24] S.S. Xantheas, J. Chem. Phys. 104 (1996) 8821.
[25] M. Schütz, S. Brdarski, P.-O. Widmark, R. Lindh, G. Karlström, J. Chem. Phys. 107 (1997) 4597.
[26] J. Sugar, C. Corliss, J. Phys. Chem. Ref. Data 10 (1981) 1097.
[27] N. Basco, S.K. Vidyarthi, D.C. Walker, Can. J. Chem. 52 (1974) 343.
[28] B.G. Ershov, E. Janata, High Energy Chem. 33 (2) (1999) 62.
[29] G.V. Buxton, R.M. Sellers, J. Chem. Soc., Faraday Trans. 1 71 (3) (1975) 558.
[30] D.F. Shriver, P.W. Atkins, C.H. Langford, Inorganic Chemistry, 2nd Edition, Oxford University Press, Oxford, 1994.
[31] P.W. Atkins, Physical Chemistry, 5th Edition, Oxford University Press, Oxford, 1994.
[32] J.H. Baxendale, E.M. Fielden, J.P. Keene, Proc. Roy. Soc. A 289 (1965) 320.
[33] M. Sanekata, F. Misaizu, K. Fuke, J. Chem. Phys. 104 (1996) 9768.
[34] M. Sanekata, F. Misaizu, F. Fuke, S. Iwata, K. Hashimoto, J. Am. Chem. Soc. 117 (1995) 747.
[35] H. Watanabe, S. Iwata, K. Hashimoto, F. Misaizu, F. Fuke, J. Am. Chem. Soc. 117 (1995) 755.